Exploring the Assembly of Supramolecular Polyoxometalate Triangular Morphologies with Johnson Solid Cores: $[(Mn^{II}(H_2O)_3)_2(K \subset \{\alpha\text{-}GeW_{10}Mn^{II}_2O_{38}\}_3)]^{19-}$
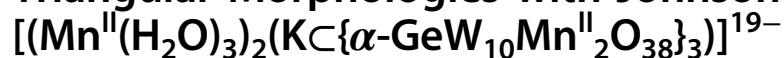
Pedro I. Molina, Haralampos N. Miras, De-Liang Long, and Leroy Cronin*

[†]WestCHEM, Department of Chemistry, The University of Glasgow, University Avenue, Glasgow G12 8QQ, Scotland, U.K.

Ⓢ Supporting Information

ABSTRACT: A new polyoxometalate (POM) cluster compound is presented which incorporates a trimeric assembly of Keggin-type germanotungstate fragments trapping a Johnson-type solid $\{Mn_8\}$ core. The mixed K−Li salt of the polyanion $[(Mn^{II}(H_2O)_3)_2(K \subset \{\alpha\text{-}GeW_{10}Mn^{II}_2O_{38}\}_3)]^{19-}$ was characterized in the solid state and solution. The correlation of the assembly processes and the observed architecture of the "trinity" family of POMs is discussed.
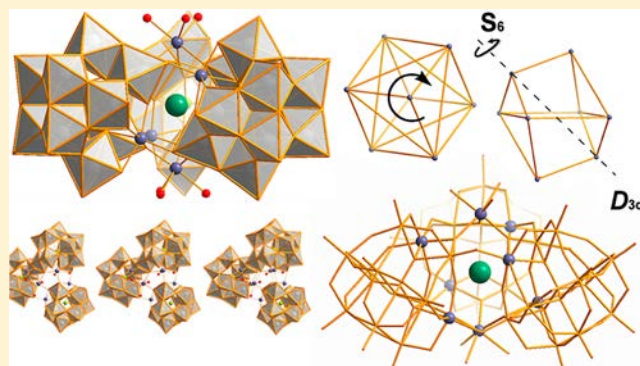
■ INTRODUCTION

Polyoxometalates (POMs) constitute a large family of anionic clusters which can be described as soluble molecular oxides of early transition metals in high oxidation state (e.g., W^{VI}, $Mo^{V/VI}$, V^V, and Nb^V).[1] Their remarkable diversity in size and topology along with their ability to incorporate a wide range of elements from the periodic table is translated in an enormous range of structural, physical and chemical properties. These features explain the sustained interest of the researchers in POM chemistry, a fact that is reflected in the near exponential increase in the number of published reports during the past 25 years that include almost every aspect of POM chemistry, from purely synthetic approaches, aimed at elucidating the assembly processes that govern POM formation, to more applied studies that seek to expand the range of applications of POMs.[2]

Transition metal substituted POMs (TMSPs) are an important subclass of the POM family. These mixed-metal polyanions can be structurally described as metal complexes where the lacunary clusters act as robust inorganic ligands. These lacunary species are typically structural derivatives of the classical POM architectures, for example, Keggin and Wells−Dawson structures.[3] TMSPs that incorporate a polynuclear, paramagnetic metallic core wrapped in a diamagnetic layer of lacunary ligands are intensely pursued as they tend to display interesting properties in the fields of molecular magnetism[4] and electrocatalysis.[5] Furthermore, their switchable redox chemistry coupled with their pronounced stability toward oxidative or hydrolytic decomposition and their inherent ability to act as Lewis acids, confers TMSPs with significant catalytic activity toward a diverse range of oxidations.[6] Moreover, a number of TMSPs have shown catalytic activity even for the thermody-

namic and kinetically demanding oxidation of water[7] although the true identity of the actual catalytic species is currently in dispute.[8]

Frustratingly, the synthetic methodologies employed are mainly based on empirical observations owing to the fact that the assembly of POMs is based on condensation processes driven by a long list of experimental variables. Consequently, the desirable achievement in POM-based systems is the fine adjustment of synthetic variables that promote the assembly of specific topology and application of rational synthetic approaches. Thus, in the synthesis of TMSPs, the most promising approach is the utilization of preformed lacunary building blocks as robust polydentate inorganic ligands under one-pot conditions in the presence of suitable electrophiles, that is, transition metal salts. From this current set of building blocks, dilacunary $\{\gamma\text{-}GeW_{10}\}$ has proved to be a most useful precursor to generate a considerable number of new mixed-metal assemblies, generally displaying interesting architectures and a wide range of nuclearities. For the above reasons, this precursor is still widely used to access new structural motifs or to elucidate the design principles of TMSP's self-assembly. In particular, $\{\gamma\text{-}GeW_{10}\}$ has been employed to generate a plethora of TMSPs resulting in numerous examples of dimeric clusters[4a,9] and interestingly, a small number of trimetric cyclical assemblies: $\{K \subset [(Ge(OH)O_3)(GeW_9Ti_3O_{38}H_2)_3]\}^{14-}$,[10] $[Rb \subset (GeW_{10}Mn_2O_{38})_3]^{17-}$ (**2**)[11] and $[(Co(H_2O)_3)(Cs \subset (GeW_{11}CoO_{38})_3]^{11-}$ (**3**),[12] see Supporting Information, Figure S1. However, it is worth noting that twice as

many cyclical trimers have been prepared using {γ-SiW$_{10}$} as precursor.[13] The observed disparity in the number of structures displaying a given topology in relation to the precursor used suggest a difference in the intrinsic reactivity and physical properties (i.e., acidity) of the lacunary species which can influence the nature of the generated building block libraries in the reaction mixture and ultimately, the final architecture of the compound. Therefore, the investigation and discovery of new TMSPs archetypes in a well-defined reaction system will increase our knowledge of the building block principles that govern the self-assembly of POM chemical systems. To that end we present herein a new member of the trimeric POM-based family, namely, $[(Mn^{II}(H_2O)_3)_2(K \subset \{\alpha$-$GeW_{10}Mn^{II}_2O_{38}\}_3)]^{19-}$ (1) (Figure 1). To the best of our knowledge, this is the first example of a trimeric transition metal substituted tungstogermanate with a {M$_8$} bicapped metallic core.
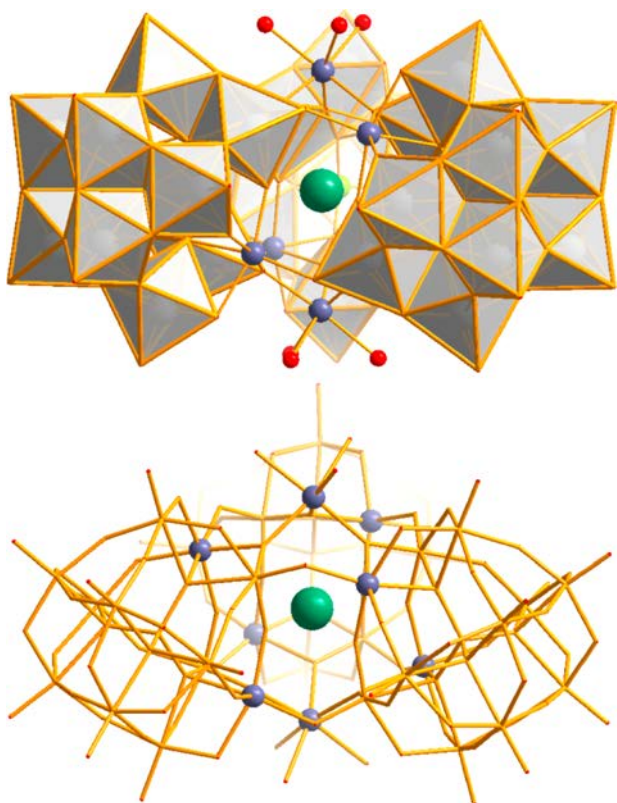

Figure 1. Top: Molecular structure of $[(Mn^{II}(H_2O)_3)_2(K \subset \{\alpha$-$GeW_{10}Mn^{II}_2O_{38}\}_3)]^{19-}$ 1. Bottom: wire frame representation of 1 highlighting the Mn centers and the central K cation. {WO$_6$}, light gray polyhedra; Mn, blue gray; Ge, light green; K, sea green; and O, red.

■ EXPERIMENTAL SECTION

General Considerations. K$_8$[γ-GeW$_{10}$O$_{36}$]·6H$_2$O was synthesized according to the published procedure.[14] All other reagents were used as purchased.

Synthesis of K$_8$Li$_{11}$[(Mn(H$_2$O)$_3$)$_2$(K⊂{α-GeW$_{10}$Mn$_2$O$_{38}$}$_3$)]·35H$_2$O. K$_8$[γ-GeW$_{10}$O$_{36}$]·6H$_2$O (0.57 g, 0.19 mmol) was added to 20 mL of 4 M aqueous LiCl under vigorous stirring. MnCl$_2$·4H$_2$O (0.10 g, 0.48 mmol) was added to the clear solution which was allowed to stir for a further 15 min. After this time, the pH of the yellow solution was increased to 7.40 by adding 1 M aqueous NaOH dropwise and then finely adjusted to 7.60 through the

slow addition of 0.5 M aqueous NaOH and maintained at 7.55−7.65 for 20 min by adding small volumes of 0.1 M aqueous NaOH. This reaction mixture was subsequently heated at 80 °C for 10 min and allowed to cool back down to room temperature under stirring. The resulting dark yellow solution (pH = 7.60) was finally transferred to a 25 mL narrow-neck conical flask and placed in a temperature-controlled crystallization room (18 ± 1 °C). Pale yellow block crystals formed from this solution overnight. The pH of the solution after removing the crystals of **1** remained within the range of 7.2−7.5.

Yield: 0.123 g, 0.013 mmol, 21% based on W. Complex Ge$_3$H$_{82}$K$_9$Li$_{11}$Mn$_8$O$_{155}$W$_{30}$, M_w = 9163.41 g mol^{-1}. Elemental analysis of the partially dehydrated material (Ge$_3$H$_{70}$K$_9$Li$_{11}$Mn$_8$O$_{149}$W$_{30}$), % (calc.): W, 60.88 (60.91); Mn, 4.32 (4.85); K, 3.87 (3.89); Li, 0.89 (0.84). Electronic absorption spectrum (UV−vis): λ(O→W) = 233 nm, ε = 9.52 × 10^4 mol^{-1} L cm^{-1}. Characteristic IR bands (cm^{-1}): 3419 (br), 1626 (sh), 1430 (sh), 1237 (m), 943 (m), 876 (sh), 783 (sh), 607(w), 444 (vw), 390 (w). Characteristic Raman bands (λ_e = 532.2 nm; ν(cm^{-1})): 880 (m), 402 (s), 326 (m), 123 (s), 88 (s). TGA water loss (25−150 °C): 6.99%.

UV−vis Spectroscopy. UV−vis spectra were recorded using a JASCO V-670 spectrophotometer in transmission mode using quartz cuvettes with 1.0 cm optical path length.

Flame Atomic Absorption Spectrometry (FAAS). W and Mn content was determined by flame atomic absorption spectroscopy (FAAS) performed on a Perkin-Elmer 1100B spectrophotometer.

Flame Photometry (FP). A Sherwood Scientific M410 INDUS-TRIAL Flame Photometer was used to determine the K and Li composition.

Fourier-Transform Infrared (FTIR) Spectroscopy. For FTIR measurements K$_8$Li$_{11}$-**1** was dispersed in a KBr pellet, and its spectrum recorded in transmission mode from a JASCO FTIR 410 spectrometer. Wavenumbers ($\tilde{\nu}$) are given in cm^{-1} while the intensities are denoted as br = broad, sh = sharp, m = medium, w = weak, and vw = very weak.

Raman Spectroscopy. Raman spectra of K$_8$Li$_{11}$-**1** crystals were collected in a Horiba Jobin-Yvon LabRAM-HR Raman microscope. The excitation wavelength was a 20 mW HeNe laser (λ = 532.2 nm).

Thermogravimetric Analysis (TGA). Thermogravimetric analysis was performed on a TA Q500 instrument from room temperature to 1000 °C at a heating rate of 5 °C min^{-1} in a N$_2$ atmosphere.

Electrochemical Experiments. Voltammograms were recorded using a Versastat 4 electro analysis system supplied by Princeton Applied Research. A standard three electrode cell was used including a Pt mesh counter electrode, a 3 mm glassy carbon working electrode and a Ag/AgCl/KCl reference electrode operating at room temperature (19 ± 1 °C). All potentials are quoted relative to the Ag/AgCl/KCl electrode. The glassy carbon working electrode was polished with diamond solution (15 μm) on nylon polishing pads, sonicated in water and then acetone before each experiment. The cell was purged with Ar for at least 15 min before each experiment.

ESI-MS Experimental Procedures and Analyses. All MS data was collected using a Q-trap, time-of-flight MS (MicrOTOF-Q MS) instrument supplied by Bruker Daltonics Ltd. The detector was a time-of-flight, microchannel plate detector, and all data was processed using the Bruker Daltonics Data Analysis 3.4 software, while simulated isotope patterns were investigated using Bruker Isotope Pattern software and Molecular Weight Calculator 6.45. The calibration solution used was Agilent ES tuning mix solution, Recorder No. G2421A, enabling calibration between approximately 100 m/z and 3000 m/z. This solution was diluted 60:1 with MeCN. Samples were introduced into the MS via direct injection at 180 μL h^{-1}. The ion polarity for all MS scans recorded was negative, at 25 °C, with the voltage of the capillary tip set at 4000 V, end plate offset at −500 V, funnel 1 RF at 300 Vpp and funnel 2 RF at 400 Vpp.

X-ray Crystallography. X-ray diffraction data was collected on an Oxford Diffraction Gemini A Ultra $[\lambda$ (Mo K_α) = 0.71073 Å] equipped with an ATLAS CCD detector. Structure solution and refinement were performed by using SHELXS-97[15] and SHELXL-97[15] integrated in the WINGX[16] system. Crystallographic data and structure refinements for (**1**): Ge$_3$H$_{82}$K$_9$Li$_{11}$Mn$_8$O$_{155}$W$_{30}$, M_W =

9163.41 g mol^{-1}; light brown crystal $0.18 \times 0.14 \times 0.08$ mm^3. Triclinic, space group $P\bar{1}$, $a = 19.5087(4)$ Å, $b = 19.8696(4)$ Å, $c = 24.1848(4)$ Å, $\alpha = 68.289(2)°$, $\beta = 68.426(2)°$, $\gamma = 63.007(2)°$. $V = 7531.5(2)$ Å^3, $Z = 2$, $T = 150$ K, $\rho = 4.041$ g cm^{-3}, 118008 reflections measured, 28561 unique ($R_{int} = 0.0644$) which were used in the calculations. Final $R1 = 0.050$ and $wR2 = 0.1247$ (all data). The data has been deposited at ICSD and given the submission number CSD-425768 at FIZ Karlsruhe, Germany, email: crysdata@fiz-karlsruhe.de.

■ RESULTS AND DISCUSSION

Reaction of divacant $\{\gamma\text{-}GeW_{10}\}$ with MnCl$_2$·4H$_2$O in an aqueous LiCl solution of high ionic strength afforded pale yellow crystals of $K_8Li_{11}[(Mn^{II}(H_2O)_3)_2(K\subset\{\alpha\text{-}GeW_{10}Mn^{II}{}_2O_{38}\}_3)]\cdot35H_2O$ (K_8Li_{11}-**1**) by overnight slow evaporation of the reaction mixture. Investigations of the self-assembly processes for the reaction mixture carried out in the pH range of 7.6−8.4 or in the presence of Na$^+$ cations, resulted in the formation of flat rhomboidal crystals of the previously reported $[Mn_4(H_2O)_2(GeW_9O_{34})_2]^{12-}$ (**4**).[17] Moreover, the mother liquor obtained after removing the crystals of **1** yielded crystals of the compound **4** during slow evaporation over a week. These observations suggest that both **1** and **4** form at a differential rate as a function of pH, as well as the remaining concentration of the transition metal providing that the rest of the synthetic parameters remain identical. Interestingly, in the absence of Li$^+$ ions only compound **4** was isolated as a pure crystalline phase. The fact that **1** forms in solution before compound **4** within a narrow pH range presumably allows for its relatively rapid crystallization as a Li/K salt.

The presence of Li$^+$, in particular, at a high concentration seems to be required for the formation of **1** as opposed to just high ionic strength; **4** is obtained as the sole product when NaCl (4M) is used as reaction medium instead of LiCl (4M) under the same experimental conditions. The small size of Li$^+$ compared to Na$^+$ cations (ionic radii: 76 pm, Li$^+$ vs 102 pm, Na$^+$) allows the concentration of a higher number of countercations around the polyanion contributing to the generation of a different set of building blocks initially in the reaction medium, to the efficient stabilization of the highly negatively charged of compound **1** (-19) in solution and finally to more efficient packing in the crystal lattice.

While the synthetic conditions under which **1**, **2**, and **3** are formed share one common feature, that is, an aqueous solutions of dilacunary precursor $\{\gamma\text{-}GeW_{10}\}$ as the starting point of the synthesis, they generally present major differences. Figure 2 summarizes the reaction coordinates for the synthetic conditions that lead to the formation of the three polyanions. The akaline metal present in all three reaction media is added both at different times and in different amounts. In the case of **1**, LiCl is added to the initial reaction mixture before the
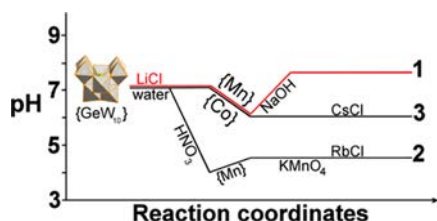
addition of any transition metal while for the synthesis of **2** and **3** the alkali metal salts (RbCl and CsCl) are added once $\{\gamma\text{-}GeW_{10}\}$ and the Mn/Co salts have already dissolved in deionized water. Furthermore, the final concentration of these alkali metals in the reaction mixture differs significantly among the three synthetic procedures: quite high for **1** and **3**, 4 and 3 M respectively, but fairly lower for **2** (0.2 M). Chloride salts of Mn/Co were used in the synthesis of **1** and **3** whereas Mn(OAc)$_2$·4H$_2$O seems to be the main source of Mn^{II} for the synthesis of compound **2**. Finally, the pH of the reaction mixture is adjusted to slightly alkaline 7.6 to afford **1** and to acidic conditions for **2** (4.5) and **3**. The alkali metals used in the syntheses of **2** and **3** appear to play a dual role; first, they seem to template the assembly of the trimeric species as they occupy the central position of the architecture, and second act as countercations, balancing out the high overall charge of the polyanions. In the case of **1**, a cooperative effect is observed between the K$^+$ and Li$^+$ cations where the Li$^+$ ions (initially present in the reaction mixture) balance the negative charge and stabilize the generated reactive intermediates, while the K$^+$ ion, supplied by the salt of the $\{\gamma\text{-}GeW_{10}\}$ precursor, contributes mainly to the templating process and less to the balancing of the remaining negative charge.

Structurally, **1** can be described in two complementary ways: as a trimeric assembly of $\{\alpha\text{-}Mn_2GeW_{10}\}$ Keggin units capped by two $[Mn(H_2O)_3]^{2+}$ centers connected to the core via $\{\mu_3\text{-}O\}$ bridges or, alternatively, as two tetrahedral $[Mn_4O_3(H_2O)_3]^{2+}$ units supported by three $[\alpha\text{-}GeW_{10}O_{36}]^{8-}$ lacunary fragments. Moreover, **1** has idealized D_{3d} symmetry where the central Mn core may be envisaged as an isomeric form of gyrobifastigium (Johnson solid, J$_{26}$)[18] in which one of the pyramids is rotated by 90° around the ideal C_3/S_6 axis passing through the $\{Mn^{II}(H_2O)_3\}$ caps and the central K$^+$ cation. Thus, this rotation changes the original D_{2d} symmetry of the regular Johnson solid to an idealized D_{3d} symmetry, Figure 3. Divacant $\{\alpha\text{-}GeW_{10}\}$ has been observed previously in only
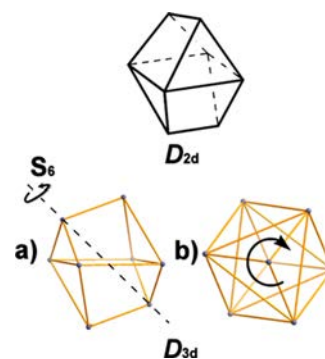

Figure 3. Top: Schematic representation of the geometry and symmetry of the regular Johnson solid (gyrobifastigium, J$_{26}$). Bottom: (a) Schematic representation of the geometry and symmetry of the irregular gyrofastidium derivative observed in **1**; (b) Representation of the core along the S$_6$ axis.

two TMSPs: **2**[11] and $\{\alpha\text{-}Fe_2GeW_{10}\}_2$,[19] the latter synthesized from trilacunary $\{\alpha\text{-}GeW_9\}$ reaction with Fe^{II} ions at a pH of 6.6, within the range of experimental conditions used for the formation of **1** and **2**. In contrast, the isolobal fragment $\{\alpha\text{-}SiW_{10}\}$ is found in considerably more TMSPs; for example, in trimetallic $\{\alpha\text{-}LnFeSiW_{10}\}_3$ (Ln = Dy, Tb)[20] which is prepared by reacting the monolacunary $\{\beta\text{-}SiW_{11}\}$ with Dy^{III} or Tb^{III} and Fe^{III} salts in the presence of ethylenediamine under hydro-

Figure 2. Representation of the synthetic parameters for the formation of **1** $[(Mn^{II}(H_2O)_3)_2(K\subset\{\alpha\text{-}GeW_{10}Mn^{II}{}_2O_{38}\}_3)]^{19-}$, **2** $Rb\subset\{\alpha\text{-}GeW_{10}Mn^{III}{}_2\ O_{38}\}_3)]^{17-}$, and **3** $[Co^{II}(H_2O)_3(Cs\subset\{\alpha\text{-}GeW_{11}Co^{II}O_{38}\}_3)]^{10-}$.

thermal conditions; or $\{\alpha\text{-Fe}_2\text{SiW}_{10}\}_2$[21] and $\{\alpha\text{-Hf}_2\text{SiW}_{10}\}_2$,[22] where the former is afforded by reacting the trilacunary $\{\alpha\text{-SiW}_9\}$ with Fe^{III} at high pH (9.2) and the latter by mixing Hf^{IV} with the dilacunary $\{\gamma\text{-SiW}_{10}\}$ at a low pH (3.6). The ability of the $\{\alpha\text{-SiW}_9\}$ moiety to incorporate an additional W center to form the $\{\alpha\text{-SiW}_{10}\}$ fragment is also demonstrated in the synthesis of $\{\text{Mn}_{19}(\alpha\text{-SiW}_{10})_6\}$, which forms in the presence of the trilacunary Keggin fragment, Mn^{II} source, and tribasic phosphate at high pH values (8.0).[23] Table 1 summarizes the reported synthetic parameters employed for the formation of the $\{\alpha\text{-M}_2\text{XW}_{10}\}$ fragment (M = first-row transition metal or lanthanide element, X = Si, Ge).

Table 1. Synthetic Parameters Employed for the Formation of the $\{\alpha\text{-M}_2\text{XW}_{10}\}$ Fragment

compound	precursor	pH	T (°C)	medium	ref
$\{\alpha\text{-Fe}_2\text{GeW}_{10}\}_2$	$\{\alpha\text{-GeW}_9\}$	6.6	80	KCl	18
$\{\alpha\text{-Mn}_2\text{GeW}_{10}\}_3$	$\{\gamma\text{-GeW}_{10}\}$	4.5	r.t.	HNO_3/Rb^+	10
$\{\alpha\text{-LnFeSiW}_{10}\}_3$ (Ln = Dy, Tb)	$\{\beta\text{-SiW}_{11}\}$	5.6	160	K_2CO_3 /Na^+	19
		5.8			
$\{\alpha\text{-Fe}_2\text{SiW}_{10}\}_2$	$\{\alpha\text{-SiW}_9\}$	9.2	80	NaOH/K^+	20
$\{\alpha\text{-Hf}_2\text{SiW}_{10}\}_2$	$\{\gamma\text{-SiW}_{10}\}$	3.6	60	AcOK/K^+	21
$\{\text{Mn}_{19}(\alpha\text{-SiW}_{10})_6\}$	$\{\alpha\text{-SiW}_9\}$	8.0	70	NaOH/ Na_3PO_4	22

A more detailed analysis of the molecular structure of **1**, **2**, and **3** allows us to make direct comparisons regarding the dimensions of their central cavity, the oxidation state of the Co/Mn centers, and the geometry of the metallic core. In **1**, the three $\{\alpha\text{-Mn}_2\text{GeW}_{10}\}$ subunits are connected by $\{Mn^{II}\text{-O-W}\}$ bridges in the same fashion as in **2** and **3** in which $\{\alpha\text{-Mn}_2\text{GeW}_{10}\}$ and $\{\text{Co}^{II}\text{GeW}_{11}\}$ subunits are linked by $\{Mn^{III}\text{-O-W}\}$ and $\{Co^{II}\text{-O-W}\}$ bridges, respectively. However, it is worth noting that while the Mn and W centers in **2** and Co and W centers in **3** are statistically disordered over the eight linkages, resulting in partial occupancies of those crystallographic positions, X-ray diffraction studies revealed full occupancy for the Mn and W positions in **1**. Bond Valence Sum (BVS)[24] analysis give an oxidation state of +2 for all the Mn centers in **1** (Supporting Information, Table T1). Furthermore, the calculations are supported by the pale yellow color of the crystals, typical of Mn^{II} compounds, and the absence of Jahn–Teller elongation in any of the Mn–O bond distances that could suggest the presence of Mn^{III} centers. Moreover, the metallic core adopts an isomeric form of the Johnson solid geometry (gyrobifastigium). On the other hand, all Mn centers in **2** are in the 3+ oxidation state, as a result of the interaction with the strong oxidizing agent ($KMnO_4$) present in the reaction mixture adopting an irregular Platonic solid geometry (octahedron), while the four Co centers in **3** are in their most usual oxidation state in POM systems, +2, and they also present an irregular Platonic solid geometry (tetrahedron). The dimensions of the metallic core incorporating the Mn or Co centers contribute to the understanding of the structural differences between **1**, **2**, and **3** (Figure 4 and Table 2). The size of the central cavity defined by the Mn or Mn/Co core (a) ranges from 7.867 Å in **1** to 7.707 Å in **3** and 7.642 Å in **2**.

Furthermore, the average distance between the "upper" and "lower" plane of the cavity defined by the M/W centers lying above and below the alkali metal ranges from 3.751 Å in **1** to
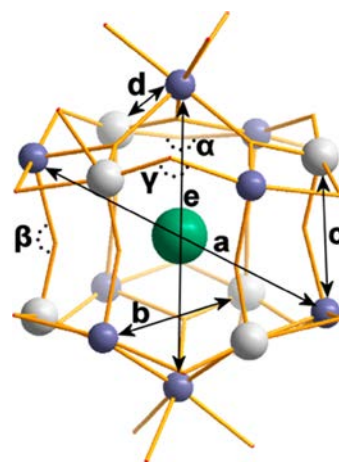

Figure 4. Schematic representation of the W/Mn core of **1**. Dimensions and angles within the core are highlighted and their average values are reported in Table 1.

Table 2. Dimensions and Angles of the Metal Center Core in 1, 2, and 3

	a(Å)	b(Å)	c(Å)	d(Å)	e(Å)	α(deg)	β(deg)
1	7.867	7.679	3.751	3.774	7.199	125	153
2	7.642	7.676	3.694			130	150
3	7.707	7.623	3.600	3.715		135	154

3.694 Å in **2** and 3.600 Å in **3**. The average diagonal distance of the cavity (b) is almost equal in **1** and **2**, 7.679 and 7.676 Å respectively, and slightly shorter, 7.623 Å, in **3**. Finally, the average distance between the metal centers at the caps and the ones in close proximity (d) is 3.774 Å in **1**, and 3.715 in **3** Å. The angle defined by Mn/Co–O–W bonds is another useful parameter for comparison purposes. The average value of the Mn/Co–O–W angle that connect the neighboring $\{\alpha\text{-Mn}_2\text{GeW}_{10}\}$ fragments (α) ranges from 125° in **1** to 130° in **2** and 135° in **3**. Moreover, the average value of the Mn/Co–O–W angle within the same $\{\alpha\text{-Mn}_2\text{GeW}_{10}\}$ unit (not shown) is almost the same in **1**, **2**, and **3**, that is, 107°, 106°, and 106°, respectively. Finally, the average value of the Mn/Co–O–W angle between the "upper" and "lower" plane (β) is 153° in **1**, 150° in **2**, and 154° in **3**. Interestingly, **1** appears to form the largest cavity with both sets of parameters (distances and angles) following a trend opposite to the ionic radii ($r_{K}^+ < r_{Rb}^+ < r_{Cs}^+$) of the templating alkali metals; additionally, the size of cavity is directly related to the number of capping metals introduced to the metallic core of the structure. The addition of each one those centers seems to increase the distance between the two planes, perpendicular to the C_3 axis formed by the W and Mn/Co, by about 0.05 Å. These observations suggest that space requirements for the coordination of the capping centers has a greater effect on the dimensions of the central cavity (forces it to expand) than the ionic radius of the templating cation.

Electrochemistry. The redox behavior of **1** was studied in aqueous solution. UV–vis stability studies in two different aqueous media and different pH values showed that compound **1** is stable long enough for the investigation of its redox properties, see Supporting Information, Figures S5 and S6. Figure 5 shows the main characteristic peaks associated with W centered redox couples in the region −0.900 V to +1.650 V of potential values vs Ag/AgCl at a scan rate of 15 mV s^{-1}. The
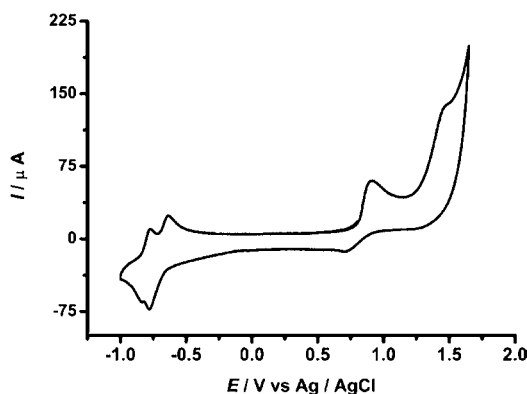
Figure 5. Cyclic voltammograms of $(2 \times 10^{-3}$ M) in aqueous 0.2 M Na_2SO_4 of 1 M CH_3COOH/CH_3COONa buffer solution (pH 4.5). The scan rate was 15 mV s^{-1}, the working electrode was glassy carbon (3 mm), and the reference electrode was Ag/AgCl.

form of the diagram remained identical no matter the scanning potential direction indicating that the phenomena observed in one domain had a negligible influence on those in the other domain. At the aforementioned scan rate and start scanning from the rest potential and moving toward the negative region of potential values, the reduction of W centers in **1** occur through two separated quasi reversible redox couples, with the corresponding $E_{1/2}$ peak potentials located at −0.709 V and −0.800 V (vs Ag/AgCl), respectively. It is well-known for the electrochemical behavior of the majority of the POMs that the number and the characteristics of these W waves depend on the pH and on the buffering strength of the electrolyte.[25−27] In the positive region of potential values, one quasireversible and one irreversible oxidation peak are observed with the $E_{1/2}$ peak potentials located at +0.810 V and +1.461 V, respectively. The simultaneous oxidation of all Mn(II) centers can be observed first, followed by an oxidation of Mn^{III} centers to Mn^{IV}. Electrolysis conducted at 1.2 and 1.6 V respectively revealed processes involving 8 ± 0.5 e^{-}. Furthermore, these data are also in good agreement with previously reported Mn−POM compounds.[11,25−27] Various cases were described in the literature for the oxidation pathways of Mn centers within POMs, with a variety of situations, including important differences in potential locations.[28,29] The characteristic sharpness of the oxidation wave indicates the presence of a surface-active species on the electrode surface. The cyclic voltammograms of **1** at different scan rates is represented in Supporting Information, Figure S2. The peak currents were proportional to the scan rate, indicating that the redox process of **1** is surface-controlled when the scan rate does not exceed the rate of 50 mV s^{-1}.

Above 100 mV s^{-1} the peak currents were proportional to the square root of the scan rate, suggesting that the redox process becomes diffusion-controlled. Broadening and overlapping of the redox couples is taking place as soon as the scan rate exceeds the value of 100 mV s^{-1} and as a consequence, important redox-related information is lost.

ESI-MS Studies. In the past decade the electrospray ionization mass spectrometry (ESI-MS) technique was used extensively by our group as analytical technique for the investigation of POM-based systems allowing us to unveil crucial information regarding the formation mechanism which takes place during the self-assembly process,[29] confirm the compound's structural integrity in solution,[30] discover new

species, and determine the extent of the metal oxide framework's protonation and composition.[31] ESI-MS studies of the of K_8Li_{11}-**1** dissolved in water confirmed that the compound retained its integrity in solution (Figure 6) during
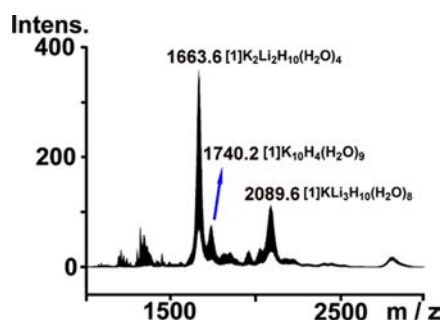

Figure 6. Negative ion mass spectrum in aqueous solution of **1**. Three envelopes of the cluster can be observed with different extent of protonation and number of counterions giving envelopes centered at m/z about 1663.6 and 1740.2 for the 5− charged species and an envelope centered at m/z about 2089.6 for the 4− charged species.

the course of the MS studies, and the observed peaks were assigned to $\{K_2Li_2H_{10}[(Mn^{II}(H_2O)_3)_2(K\subset\{\alpha\text{-}GeW_{10}Mn^{II}_2O_{38}\}_3)](H_2O)_4\}^{5-}$, $\{K_{10}H_4[(Mn^{II}(H_2O)_3)_2\text{-}(K\subset\{\alpha\text{-}GeW_{10}Mn^{II}_2O_{38}\}_3)](H_2O)_9\}^{5--}$ and $\{KLi_3H_{10}\text{-}[(Mn^{II}(H_2O)_3)_2(K\subset\{\alpha\text{-}GeW_{10}Mn^{II}_2O_{38}\}_3)](H_2O)_8\}^{4-}$ giving envelopes centered at m/z about 1663.6, 1740.2, and 2089.6 respectively.

■ CONCLUSIONS

We have shown that the thorough investigation of the parameter space of POM-based systems is crucial for the discovery and isolation of new species and for the entrapment of new metallic cores. The self-assembly process was directed by the cooperative effect of the alkali metals present in solution, the pH value, and the ionic strength of the reaction mixture which allowed the isolation of a new member of the "trinity" family of POMs which traps and stabilizes an irregular $\{Mn_8\}$ Johnson solid type and exhibits the formula $[(Mn^{II}(H_2O)_3)_2(K\subset\{\alpha\text{-}GeW_{10}Mn^{II}_2O_{38}\}_3)]^{19-}$ (**1**). In this work the above compound was studied extensively in solid state by X-ray diffraction as well as in solution by ESI-MS which allowed us to demonstrate the compound's structural integrity in solution. Furthermore, X-ray diffraction studies showed that the size of the formed cavity (S) is directly related to the number of capping transition metal centers and not to the ionic radius of the alkali metal template. For this reason the size of the cavity for the clusters **1**−**3** ($S_1 > S_2 > S_3$) follows an opposite trend to the ionic radii ($r_K^+ < r_{Rb}^+ < r_{Cs}^+$) of the templating alkali metals. Careful, investigation of the $[GeW_{10}O_{36}]^{8-}/M^{n+}$ system showed the efficiency of the POM-lacunary species as inorganic ligands for the entrapment of different nuclearities and symmetries of solids ranging from Platonic, $\{M_6\}$ octahedron and $\{M_4\}$ tetrahedron, to highly symmetrical (D_{3d}) irregular Johnson solids such as the $\{M_8\}$ gyrobifastigium derivative, see Supporting Information, Figure S3. Moreover, the electrochemical studies in aqueous media showed well separated redox waves for the oxidation of the Mn^{II} metal centers in the region of 0.500 V−1.600 V and a typical set of two quasi-reversible redox couples in the region −0.500 V to −1.000 V for the W centered reductions respectively.

All these observations indicate that the {GeW$_{10}$} precursor has a tremendous potential for generation of novel building block libraries which can lead to the discovery of new compounds which incorporate metallic cores with interesting geometries, redox and magnetic properties with potential applications in catalysis, electronic materials, and devices. In further work, we will try and expand our investigations on the {GeW$_{10}$O$_{36}$}$^{8-}$/M^{n+} system by trapping metallic cores of different geometries to finely tune their magnetic, electronic, and catalytic properties and correlate the adopted geometry with the observed functionality.

ASSOCIATED CONTENT

ⓈSupporting Information

The ESI-MS, CV, structural, and spectroscopic details. This material is available free of charge via the Internet at http://pubs.acs.org.

AUTHOR INFORMATION

Corresponding Author

*E-mail: L.Cronin@chem.gla.ac.uk. Phone: +44 (0)141 330 6650. Fax: +44 141 330 4888. Website: http://www.chem.gla.ac.uk/staff/lee or http://www.croninlab.com.

Notes

The authors declare no competing financial interest.

ACKNOWLEDGMENTS

REFERENCES

(1) Miras, H. N.; Yan, J.; Long, D.-L.; Cronin, L. *Chem. Soc. Rev.* **2012**, *41*, 7403.

(2) (a) Long, D.-L.; Tsunashima, R.; Cronin, L. *Angew. Chem., Int. Ed.* **2010**, *49*, 2. (b) Song, Y.-F.; Tsunashima, R. *Chem. Soc. Rev.* **2012**, *41*, 7384.

(3) (a) Long, D.-L.; Burkholder, E.; Cronin, L. *Chem. Soc. Rev.* **2007**, *36*, 105. (b) Oms, O.; Dolbecq, A.; Mialane, P. *Chem. Soc. Rev.* **2012**, *41*, 7497.

(4) (a) Ritchie, C.; Ferguson, A.; Nojiri, H.; Miras, H. N.; Song, Y.-F.; Long, D.-L.; Burkholder, E.; Murrie, M.; Kögerler, P.; Brechin, E. K.; Cronin, L. *Angew. Chem., Int. Ed.* **2008**, *47*, 5609. (b) Ibrahim, M.; Lan, Y.; Bassil, B. S.; Xiang, Y.; Suchopar, A.; Powell, A. K.; Kortz, U. *Angew. Chem., Int. Ed.* **2011**, *50*, 4708.

(5) Keita, B.; Nadjo, L. *J. Mol. Catal. A* **2007**, *262*, 190.

(6) Mizuno, N.; Kamata, K.; Yamaguchi, K. *Top. Organomet. Chem.* **2011**, *37*, 127.

(7) (a) Sartorel, A.; Carraro, M.; Scorrano, G.; De Zorzi, R.; Geremia, S.; McDaniel, N. D.; Bernhard, S.; Bonchio, M. *J. Am. Chem. Soc.* **2008**, *130*, 5006. (b) Geletii, Y. V.; Botar, B.; Kögerler, P.; Hillesheim, D. A.; Musaev, D. G.; Hill, C. L. *Angew. Chem., Int. Ed.* **2008**, *47*, 3896. (c) Yin, Q.; Tan, J. M.; Besson, C.; Geletii, Y. V.; Musaev, D. G.; Kutnetsov, A. E.; Luo, Z.; Hardcastle, K. I.; Hill, C. L. *Science* **2010**, *328*, 342. (d) Zhu, G.; Geletii, Y. V.; Kögerler, P.; Schilder, H.; Song, J.; Lense, S.; Zhao, C.; Hardcastle, K. I.; Musaev, D. G.; Hill, C. L. *Dalton Trans.* **2012**, *41*, 2084.

(8) Stracke, J. J.; Finke, R. G. *J. Am. Chem. Soc.* **2011**, *133*, 14872.

(9) (a) Nsouli, N. H.; Mal, S. S.; Dickman, M. H.; Kortz, U.; Keita, B.; Nadjo, L.; Clemente-Juan, J. M. *Inorg. Chem.* **2007**, *46*, 8763. (b) Nsouli, H. N.; Ismail, A. H.; Helgadottir, I. S.; Dickman, M. H.; Clemente-Juan, J. M.; Kortz, U. *Inorg. Chem.* **2009**, *48*, 5884. (c) Nsouli, N. H.; Prinz, M.; Damnik, N.; Neumann, M.; Talik, E.; Kortz, U. *Eur. J. Inorg. Chem.* **2009**, *34*, 5096. (d) Tan, R.; Li, D.; Wu,

H.; Zhang, C.; Wang, X. *Inorg. Chem. Commun.* **2008**, *11*, 835. (e) Zhang, Z.; Wang, E.; Li, Y.; Qi, Y.; Tan, H. *J. Mol. Struct.* **2007**, *843*, 128. (f) Zhang, Z.; Wang, E.; Li, Y.; An, H.; Qi, Y.; Xu, L. *J. Mol. Struct.* **2008**, *872*, 176. (g) Zhang, Z.; Yao, S.; Wang, E.; Shi, Q.; Zhang, H. *J. Cluster Sci.* **2008**, *19*, 521.

(10) Ren, Y.-H.; Liu, S.-X.; Cao, R.-G.; Zhao, X.-Y.; Cao, J.-F.; Gao, C.-Y. *Inorg. Chem. Commun.* **2008**, *11*, 1320.

(11) Mitchell, S. G.; Khanra, S.; Miras, H. N.; Boyd, T.; Long, D.-L.; Cronin, L. *Chem. Commun.* **2009**, 2712.

(12) Chen, L.; Shi, D.; Zhao, J.; Wang, Y.; Ma, P.; Wang, J.; Niu, J. *Cryst. Growth Des.* **2011**, *11*, 1913.

(13) (a) Kortz, U.; Matta, S. *Inorg. Chem.* **2001**, *40*, 815. (b) Al-Kadamany, G. A.; Hussain, F.; Mal, S. S.; Dickman, M. H.; Leclerc-Laronze, N.; Marrot, J.; Cadot, E.; Kortz, U. *Inorg. Chem.* **2008**, *47*, 8574. (c) Mialane, P.; Dolbecq, A.; Marrot, J.; Rivière, E.; Sécheresse, F. *Chem.—Eur. J.* **2005**, *11*, 1771. (d) Botar, B.; Geletii, Y. V.; Kögerler, P.; Musaev, D. G.; Morokuma, K.; Weinstock, I. A.; Hill, C. L. *J. Am. Chem. Soc.* **2006**, *128*, 11268. (e) Mitchell, S. G.; Ritchie, C.; Long, D.-L.; Cronin, L. *Dalton Trans.* **2008**, 1415.

(14) Nsouli, H. N.; Bassil, B. S.; Dickman, M. H.; Kortz, U.; Keita, B.; Nadjo, L. *Inorg. Chem.* **2006**, *45*, 3858.

(15) Sheldrick, G. M. *Acta Crystallogr., Sect. A: Found. Cryst.* **2008**, *64*, 112.

(16) Farrugia, L. J. *J. App. Crystallogr.* **1999**, *32*, 837.

(17) Kortz, U.; Nellutla, S.; Stowe, A. C.; Dalal, N. S.; Rauwald, U.; Danquah, W.; Ravot, D. *Inorg. Chem.* **2004**, *43*, 2308.

(18) Johnson, N. W. *Can. J. Math.* **1966**, *18*, 169.

(19) Liu, Y.; Shang, J.; Xue, G.; Hu, H.; Fu, F.; Wang, J. *J. Cluster Sci.* **2007**, *18*, 205.

(20) Zhang, Z.-M.; Li, Y.-G.; Yao, S.; Wang, E.-B. *Dalton Trans.* **2011**, *40*, 6475.

(21) Zhao, X.; Li, Y.-G.; Wang, Y.-H.; Wang, E.-B. *Transition Met. Chem.* **2008**, *33*, 323.

(22) Assran, A. S.; Mal, S. S.; Izarova, N. V.; Banerjee, A.; Suchopar, A.; Sadakane, M.; Kortz, U. *Dalton Trans.* **2011**, *40*, 2920.

(23) Bassil, B. S.; Ibrahim, M.; Al-Oweini, R.; Asano, M.; Wang, Z.; Van Tol, J.; Dalal, N. S.; Choi, K.-Y.; Biboum, R. N.; Keita, B.; Nadjo, L.; Kortz, U. *Angew. Chem., Int. Ed.* **2011**, *50*, 5961.

(24) Brown, I. D. *J. Appl. Crystallogr.* **1996**, *29*, 479.

(25) (a) Bi, L. H.; Wang, E.-B.; Peng, J.; Huang, R. D.; Xu, L.; Hu, C. W. *Inorg. Chem.* **2000**, *39*, 671. (b) Mbomekalle, I. M.; Keita, B.; Nadjo, L.; Berthet, P.; Neiwert, W. A.; Hill, C. L.; Ritorto, M. D.; Anderson, T. M. *Dalton. Trans.* **2003**, 2646. (c) Contant, R.; Abbessi, M.; Canny, J.; Richet, M.; Keita, B.; Belhouari, B.; Nadjo, L. *Eur. J. Inorg. Chem.* **2000**, 567.

(26) (a) Mitchell, S. G.; Streb, C.; Miras, H. N.; Boyd, T.; Long, D.-L.; Cronin, L. *Nat. Chem.* **2010**, 308. (b) Boyd, T.; Mitchell, S. G.; Miras, H. N.; Long, D.-L.; Cronin, L. *Dalton Trans.* **2010**, 6460.

(27) (a) Mitchell, S. G.; Molina, P. I.; Khanra, S.; Miras, H. N.; Prescimone, A.; Cooper, G. J. T.; Winter, R. S.; Brechin, E. K.; Long, D.-L.; Cogdell, R. J.; Cronin, L. *Angew. Chem., Int. Ed.* **2011**, *50*, 9154. (b) Keita, B.; Mbomekalle, I. M.; Lu, Y. W.; Nadjo, L.; Berthet, P.; Anderson, T. M.; Hill, C. L. *Eur. J. Inorg. Chem.* **2004**, 3462.

(28) Liu, J.; Ortega, F.; Sethuraman, P.; Katsoulis, D. E.; Costello, C. E.; Pope, M. T. *J. Chem. Soc., Dalton Trans.* **1992**, 1901.

(29) Bosing, M.; Noh, A.; Loose, I.; Krebs, B. *J. Am. Chem. Soc.* **1998**, *120*, 7252.

(30) (a) Miras, H. N.; Wilson, E. F.; Cronin, L. *Chem. Commun.* **2009**, 1297. (b) Wilson, E. F.; Miras, H. N.; Rosnes, M. H.; Cronin, L. *Angew. Chem., Int. Ed.* **2011**, *50*, 3720.

(31) (a) Miras, H. N.; Stone, D. J.; McInnes, E. J. L.; Raptis, R. G.; Baran, P.; Chilas, G. I.; Sigalas, M. P.; Kabanos, T. A.; Cronin, L. *Chem. Commun.* **2008**, 4703. (b) Miras, H. N.; Yan, J.; Long, D.-L.; Cronin, L. *Angew. Chem., Int. Ed.* **2008**, *47*, 8420.

(32) (a) Song, Y.-F.; Long, D.-L.; Kelly, S. E.; Cronin, L. *Inorg. Chem.* **2008**, *47*, 9137. (b) Miras, H. N.; Ochoa, M. N. C.; Long, D.-L.; Cronin, L. *Chem. Commun.* **2010**, *46*, 8148.